NanoImpact 17 (2020) 100195

Contents lists available at ScienceDirect

NanoImpact

journal homepage: www.elsevier.com/locate/nanoimpact

Hazard assessment of polymer-capped CuO and ZnO nanocolloids: A contribution to the safe-by-design implementation of biocidal agents

Luisa Fiandra[a,*,1], Patrizia Bonfanti[a,1], Ylenia Piunno[a], Anjani P. Nagvenkar[b], Ilana Perlesthein[b], Aharon Gedanken[b], Melissa Saibene[a], Anita Colombo[a], Paride Mantecca[a]

[a] POLARIS Research Centre, Dept. Of Earth and Environmental Sciences, University of Milano – Bicocca, Milano, Italy
[b] Department of Chemistry, Institute of Nanotechnology and Advanced Materials, Bar-Ilan University, Israel

ARTICLE INFO

Keywords:
MeO antibacterial nanoparticle
Cytotoxicity
Xenopus laevis
Developmental toxicity
FETAX

ABSTRACT

The antibacterial activity of metal oxide (MeO) nanoparticles (NPs) has been extensively reported. Nevertheless, there is a general concern about MeO NPs toxicity, and much efforts are being devoted to improve a safe employment of these nanomaterials by surface functionalization. In this work, we propose to investigate if the coating of copper and zinc oxides (CuO and ZnO) NPs with the polymers poly(ethylene imine) (PEI) or poly (ethylene glycol) (PEG) is able protect non-target cells and organisms from the toxicity of antibacterial MeOs NPs. The overall results obtained exposing lung cells and *Xenopus laevis* embryos to CuO-PEG, CuO-PEI, ZnO-PEG and ZnO-PEI, indicate that PEG, but not PEI coating, is able to exert a protective function against MeOs toxicity. The ability of PEG shell to reduce the adverse impact of MeOs NPs is in part associated to a protection from the oxidative stress, even if in vitro results indicate that peghylation is not able to prevent pro-inflammatory responses. We suggest that the different intracellular availability of the metal oxides upon capping with PEG or PEI, together with the involvement of multiple mechanisms of action, may be responsible for the different toxicological outcome on lung cells viability and *Xenopus* mortality and malformations.

1. Introduction

Metal oxide (MeO) nanoparticles (NPs) have been widely described as valid antibacterial tools in several fields of applications (pharmacy, food packaging, medical textile coating, etc.). Different experimental approaches, employed to assess the high potential of these nanoparticles against bacteria, highlighted the importance of their chemical-physical features and the involvement of multiple modes of action in determining their antibacterial efficiency (Kadiyala et al., 2018).

Among MeO NPs, those based on copper oxide (CuO) and zinc oxide (ZnO) have been proved highly effective against different strains of bacteria (Azam et al., 2012; Perelshtein et al., 2015a) and they have been identified as promising bactericidal devices for food industry (He and Hwang, 2016) and nosocomial infections (Perelshtein et al., 2015b).

Despite the high potential of copper- and zinc-based NPs as antibacterial materials, their toxicity still today limits their use. It has been described as metal oxide nanoparticles, including CuO and ZnO NPs, exert a strong cytotoxic impact in vitro, mainly due to Reactive Oxygen Species (ROS) production and genotoxicity subsequent to their internalization (Akhtar et al., 2016; Chang et al., 2012; Kung et al., 2015). Moreover, MeOs dissolution and a direct impact on cell membrane seem to play a key role in NPs adverse effects (Chang et al., 2012; Ivask et al., 2014). In our previous works, we have extensively studied and compared the toxic effect of different commercial and sonochemically synthetized CuO and ZnO NPs on the early development of *Xenopus laevis* (Bacchetta et al., 2013; Bonfanti et al., 2015; Mantecca et al., 2015; Perelshtein et al., 2015a), which have been successfully proposed as a suitable model to evaluate the toxicity of nanostructured metal oxides on live organisms (Bacchetta et al., 2012; Nations et al., 2011). The results of these studies highlighted that CuO NPs displayed an embryotoxic potential only at high concentrations (> 100 mg/L), mainly attributable to ions dissolved by NPs, while ZnO NPs themselves showed different degrees of embryotoxicity, depending on their shape and size, specifically targeting gut development and causing abdominal and cardiac edema.

Surface functionalization of MeOs with polymeric shell has been identified as a powerful strategy to increase the stability of the colloidal solution, which in turn affects the antibacterial efficiency of the nanomaterials (Nagvenkar et al., 2016). It is therefore feasible that

* Corresponding author.
E-mail address: luisa.fiandra@unimib.it (L. Fiandra).
[1] Equally contributed to the work.

https://doi.org/10.1016/j.impact.2019.100195
Received 7 June 2019; Received in revised form 31 October 2019; Accepted 8 November 2019
Available online 21 November 2019

engineering of MeO NPs surface could also reduce their toxicity towards non-target cells and live organisms. Surface coating has been already proposed as a promising strategy to reduce metal oxide-NPs cytotoxicity (Cai et al., 2017; Osmond McLeod et al., 2014).

In the present study, we focused on the safety profile of CuO and ZnO NPs coated with poly(ethylene imine) (PEI) and poly(ethylene glycol) (PEG) by a one-step ultrasound-based technique. The synthesis and characterization of these PEI- and PEG-capped MeO nanocolloids have been recently reported by Nagvenkar et al. (Nagvenkar et al., 2019), who described the high stability of these functionalized metal oxides and its positive influence on NPs antibacterial activity. Our study aimed to perform an extensive safety assessment of CuO- and ZnO-PEG/PEI nanocolloids, combining standardized in vitro protocols on human lung cells with the model of early developmental vertebrate *Xenopus laevis*. Investigated by means of Frog Embryo Teratogenesis Assay-Xenopus (FETAX).

2. Results and discussion

2.1. Characterization of doped NPs

CuO-PEG, CuO-PEI, ZnO-PEG and ZnO-PEI, synthetized according to a previously described protocol,15,18 have been characterized in shape, size and surface charge. Trasmission Electron Microscopy (TEM) images (Fig. 1) showed the same fibrous or nearly spherical shape for coated CuO and ZnO NPs, respectively, typical of the corresponding non-doped NPs. The TEM-derived primary size of CuO and ZnO NPs was similar in the PEI- and PEG-derivates, while the hydrodynamic diameter of both MeOs in water, and of CuO NPs in cell medium, was higher upon functionalization with PEG than that obtained with PEI. The hydrodynamic diameter in Fetax solution is almost the same for the four nanoparticle types. Z potential was positive and comparable in CuO and ZnO NPs (Table 1).

2.2. Effect of PEI and PEG capping on CuO and ZnO NPs in vitro cytotoxicity

Cytotoxicity of CuO and ZnO NPs has been assessed in the widely described A549 human lung epithelial cells (Sahu et al., 2013). Although Air Liquid Interface (ALI) has been recently approved as a valid alternative method to the submerged system in studying the biological effects of engineered nanoparticles (Lenz et al., 2013), in the present work we preferred to use a simplified 2D culture of A549 cells in order to maintain the same dispersion method of NPs employed for the live animal assays and obtain the same controlled nanoparticle concentration in cell medium of Xenopus treatment solutions. Moreover, A549 culture is a well-standardized method employed as main model for several biological endpoints in the context of the NANoREG framework for the safety assessment of nanomaterials (Van Teunenbroek, 2016). Limitation in using submerge exposure respect to ALI can be related to being in a condition more distant to the real exposure scenario (i.e. different bioavailability to O_2, different interaction with NPs in the absence of a lining fluid).

In a previous work, we had already demonstrated the impact of high dosages of sonochemically produced CuO and ZnO NPs on A459 lung cells by assessing their viability and interleukin production (Mantecca et al., 2017). Moreover, in a more recent study we reported preliminary viability assays that documented the ability of PEG-coated CuO NPs to induce a much lower cytotoxicity on lung cells respect to the naked nanoparticles (Nagvenkar et al., 2019). To evaluate if the coating of

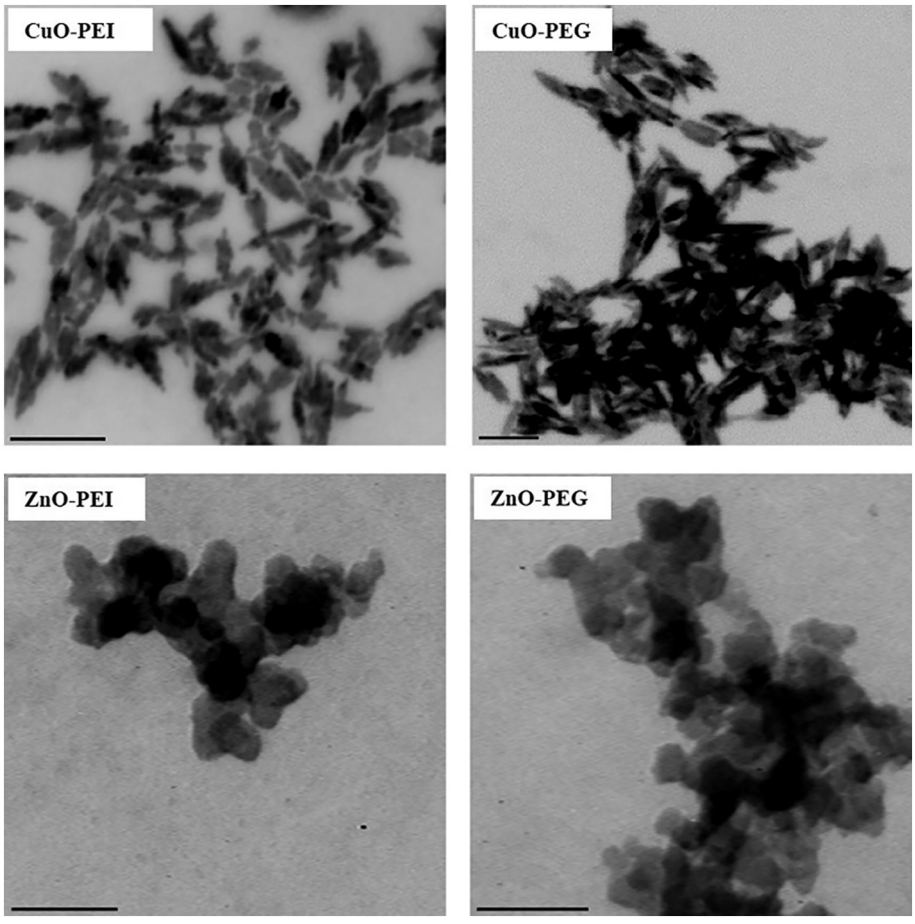

Fig. 1. Transmission electron microscopy (TEM) images of CuO-PEI/PEG and ZnO-PEI/PEG. Bar: 100 nm.

Table 1
Characterization of CuO-PEI/PEG and ZnO-PEI/PEG NPs. Primary size as derived from TEM images. *Z*-potential as measured by dynamic light scattering (DLS) in water. Hydrodynamic size and polydispersity index (Pdl) as measured by DLS in water, cell medium and Fetax solution. Means ± SE of 5 replicates.

	CuO-PEI	CuO-PEG	ZnO-PEI	ZnO-PEG
Primary size (nm)	60–50 (length) 20–30 (width)	70–80 (length) 10–20 (width)	50–80	40–60
Z-potential (mV)	37.1 ± 0.46	14.8 ± 0.60	44.1 ± 0.69	11 ± 1.08
	Hydrodynamic diameter (nm) ± SE (PdI)			
Water	1428 ± 44 (0.40)	3107 ± 246 (0.45)	487 ± 47 (0.60)	1839 ± 59 (0.38)
Cell medium	1409 ± 85 (0.31)	2087 ± 63 (0.27)	1891 ± 108 (0.49)	1971 ± 109 (0.22)
Fetax solution	1993 ± 71 (0.32)	2005 ± 26 (0.19)	2529 ± 52 (0.11)	2004 ± 24 (0.26)

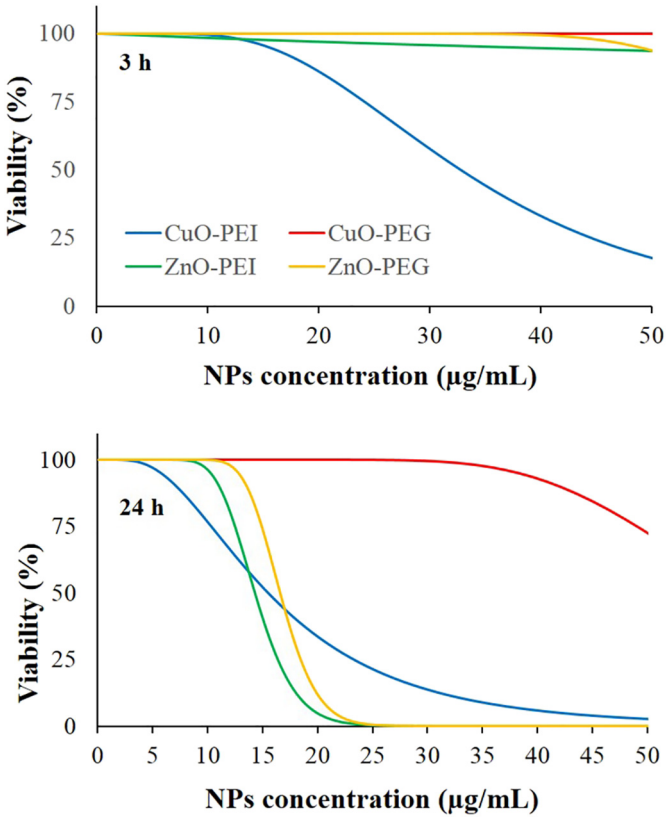

Fig. 2. Cell viability evaluated by MTT test after 3 h (A) or 24 h (B) exposure to increasing doses of CuO-PEG, CuO-PEI, ZnO-PEG and ZnO-PEI NPs. Curves represent the percentage (%) of cell viability respect to the control sample (untreated cells, cells viability 100%).

Table 2
EC50 values (µg/mL) for cell viability assay (EC50: effective concentration of compound decreasing cell viability by 50%). Mean ± SD.

	CuO-PEI	CuO-PEG	ZnO-PEI	ZnO-PEG
3 h	32.8 ± 0.45	ND	ND	69.9 ± 0.22
24 h	15.5 ± 0.6	58.3 ± 0.26	14.3 ± 0.2	16.6 ± 0.16

ND = Not detectable.

PEG and PEI could protect A549 cells from CuO and ZnO NPs cytotoxicity, a dose-response evaluation of cell viability was assessed at 3 and 24 h of incubation with CuO-PEG, CuO-PEI, ZnO-PEG and ZnO-PEI (Fig. 2 and S1). CuO-PEI induced cytotoxicity already after 3 h of treatment at concentrations higher than 10 µg/mL, while CuO-PEG and all coated ZnO NPs showed no significant effects respect to control at 3 h. At 24 h a severe cytotoxic effect was observed with CuO-PEI and all coated ZnO NPs, but not with CuO-PEG. The delayed effect of both PEG- and PEI-ZnO is in line with previous studies describing the time-dependent cytotoxicity of this metal oxide. In detail, no significant effect on cell viability were recorded at 2 h of tratment with > 20 µg/mL ZnO NPs, but a much higher significant response was observed strarting from six hours of incubation, reaching a potent viability decrease at 24 h (Liu et al., 2017). EC50 values derived from viability curves (Table 2) clearly indicate that while PEG coating was able to protect cells from the cytotoxic impact of CuO (EC50 of CuO-PEG NPs is 3.8-fold higher than that of CuO-PEI), the same protection was not obtained on ZnO NPs.

To better understand the role of the two polymeric coatings on CuO and ZnO NPs cytotoxicity, the production of ROS was then determined at 3 and 6 h of incubation with the nanoparticles, starting from the concentration effective on cell viability (20 µg/mL). While no difference with respect to control was observed in A549 cells exposed for 3 h to all the examined nanoparticles, except for a small increase in the presence of ZnO-PEI NPs, a more significant effect was detected after 6 h of incubation (Fig. 3).

In particular, in cells treated with CuO-PEI NPs, the oxidative stress was strongly increased compared to control in a concentration-dependent manner, and a significant effect was also observed in the cells exposed to doses of ZnO-PEI higher than 25 µg/mL. Therefore, the ability of PEG coating to reduce CuO NPs toxicity was confirmed, since no oxidative stress was observed in the cells treated with 20 and 25 µg/mL CuO-PEG, and the ROS production in the presence of CuO-PEG NPs was significantly lower than that recorded with the same concentrations of CuO-PEI. The analogue protective role of PEG on A549 oxidative stress was also observed with zinc oxide nanoparticles (Fig. 3).

We assumed that the increased protection from oxidative stress in the cells exposed to PEGylated MeOs, together with the lower cytotoxicity of PEG- vs. PEI-coated CuO NPs was related to the different rate of endocytosis of the two coating components, which in turn affects the amount of internalized nanoparticles. Indeed, PEI is known to be efficiently translocated in A549 cells both by clathrin-mediated and by caveolae-mediated endocytosis (Rejman et al., 2005), thanks to its highly positive surface charge. To verify this hypothesis, an ICP-OES quantification of Cu and Zn content in cells incubated for 24 h with the four NP types was performed. Table 3 shows that zinc accumulation in cells is not affected by the different polymeric shell, and even the intracellular content of Cu^{2+} after incubation with PEG-coated CuO is higher than that measured after CuO-PEI exposure.

Therefore, a comparable amount of PEI- and PEG- NPs seems to be internalized by lung cells and reach the lysosomes to be subjected to enzymatic degradation. Nevertheless, the amount of uncoated NPs and free Cu^{2+} and Zn^{2+} resulting from CuO/ZnO-PEI depletion and escaping from lysosomes into the cytoplasm would be larger than that obtained from CuO/ZnO-PEG, due to the "proton sponge" effect. This process is typical of PEI-functionalized materials (Behr, 1997) which can be therefore released from the lysosomes in to the cytoplasm with a much higher extent. As a result, a higher extent of CuO and ZnO and dissolved Cu^{2+} and Zn^{2+} would be available to interact with mitochondria and activate ROS production upon release from PEI-coated NPs, respect to what obtained with PEG-coated NPs (Scheme 1).

Up to this point, we conclude that while PEG coating is able to

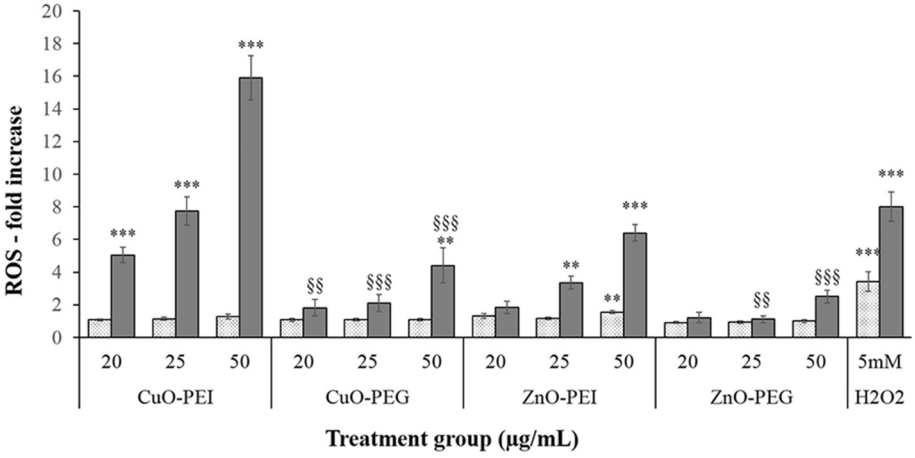

Fig. 3. Intracellular ROS fold-increase in A549 cells after 3 (light grey) and 6 h (dark grey) from treatment with CuO-PEG, CuO-PEI, ZnO-PEG and ZnO-PEI NPs at increasing concentrations (20–50 µg/mL), compared to untreated cells (solid line). Mean ± SE of 4 replicates. ***$p < 0.001$, **$p < 0.01$, vs. control (One-way ANOVA); §§§$p < 0.001$, §§$p < 0.01$ (Student *t*-test) vs. corresponding PEI-coated NP.

Table 3
Bioaccumulation of Cu^{2+} and Zn^{2+} in embryos exposed to 20 µg/mL CuO-PEI, CuO-PEG, ZnO-PEI and ZnO-PEG. The values, expressed as µg/mL x 10^6 and normalized on the n° of cells at the end of incubation, are reported as Mean ± SE of 3 independent ICP-OES analyses.

	CuO-PEI	CuO-PEG	ZnO-PEI	ZnO-PEG
Cu^{2+}	0.59 ± 0.08	1.29 ± 0.02	–	–
Zn^{2+}	–	–	1.85 ± 0.37	2.08 ± 0.16

protect A549 cells from the metal oxide-induced oxidative stress, the coating with PEI of both CuO- and ZnO was totally unable to prevent ROS production. A long-time effect on cell viability was observed only with CuO-PEG, while the low ROS content in the cells exposed to ZnO-PEG does not prevent metal oxide-induced cell death (Fig. 3). To clarify the contribution of oxidative stress in MeOs-PEI/PEG- related cytotoxicity, the release of the pro-inflammatory cytokine interleukin-8 (IL-8) was also investigated. IL-8 gene transcription in lung cells is known to be up-regulated by exposure to metal oxide nanoparticles, thanks to the ROS-mediated activation of nuclear factor-kappa B and mitogen-activated protein kinase (Khanna et al., 2015). A549 cells were exposed for 24 h to increasing concentration of MeOs-PEG and -PEI. Fig. 4 shows that treated cells were able to release IL-8 at a higher amount than control cells, following a dose-response trend from 1 to 50 µg/mL. The dose of 20 µg/mL represented the most effective for CuO-PEI, ZnO-PEG and ZnO-PEI, while CuO-PEG activity increased up to 50 µg/mL. The gaussian trend of IL-8 released from the cells exposed to CuO-PEI, ZnO-PEG and ZnO-PEI could be the result of the high cell death percentage in these samples over 24 h, not observed in the cells exposed to CuO-PEG (Fig. 2). A full relationship between oxidative stress and cytokines release was not observed. In particular, the two pegylated NPs and ZnO-PEI, which induced a significant increase of IL-8 release at 20 µg/mL, were uneffective on the oxidative stress at the same dose (Fig. 3). It is important to highlight that, not only a ROS-mediated cytotoxicity, but also a direct interaction of MeOs NPs with DNA can occur in treated cells, due to their permeation across nucleopores (Hou et al., 2017; Scherzad et al., 2017; Wang et al., 2012). Therefore, a mechanism of action not including the oxidative stress, but associated to the nuclear accumulation of the MeOs NPs, is likely responsible for the high pro-inflammatory cytokine release in all samples (Scheme 1). Non-dissociated MeOs would be mainly involved in the ROS-independent cytotoxicity, since previous studies had demonstrated a negligible direct effect of dissolved ions on DNA, respect to a much more significant contribution on the oxidative stress (Midander et al., 2009).

The outcome of CuO and ZnO NPs on A549 viability is hence the result of the relative contribution of ROS-dependent and -independent cytotoxic mechanisms, differently involved by the two polymeric coatings. In this sense, the adverse effect of ZnO-PEG NPs on cell viability, without affecting the oxidative status, can be due to the direct impact of ZnOs on DNA, apparently stronger than that exerted by CuOs.

We cannot exclude that a certain cytotoxicological impact would be also induced by the ions released into extracellular medium during the incubation with the NPs. Our preliminary studies, demonstrated that 25 ppm CuO and ZnO NP are able to release the 50% of ions after 24 h in medium (data not shown). We have now confirmed an analogue percentage also with PEI- and PEG-ZnO NPs and about 80% with coated CuO NPs (Table S1). Nevertheless, since no differences in the amount of released ions have been observed between the two shell types, we did not retain necessary highlight the contribution of extracellular ions in the present work.

2.3. Assays on a whole developing vertebrate

In recent years, Xenopus embryos have been accepted as ideal model to evaluate the developmental toxicity of nanostructured metal oxides (Bacchetta et al., 2012; Marín-Barba et al., 2018; Nations et al., 2011). In the present work, the FETAX has been used to evaluate if the PEI and PEG coatings affect the developmental toxicity of sonochemically produced CuO and ZnO antibacterial NPs.

At the end of FETAX test, the results showed that both ZnO-PEI and -PEG NPs were not embryolethal at all tested concentrations (10–50 µg/mL). On the contrary, a big difference between the CuO-PEG and -PEI NPs was highlighted, as the latter caused a drastic increase in the mortality rate at a concentration of 10 µg/mL (Fig. 5A).

The CuO-PEI median 96 hpf LC50 calculated by Probit analysis was indeed 7,5 µg/mL (Table 4). The embryolethality of CuO-PEI was of particular significance considering that none of naked CuO NPs previously tested in *Xenopus laevis* embryos induced mortality even at concentrations higher than 50 µg/mL.13,14,12 Similarly, in developing zebrafish different commercial and green synthetized CuO NPs yielded LC50 values ranging from 45 to 175 µg/mL (Ganesan et al., 2016; Kumari et al., 2017), and no effect on zebrafish phenotypes at a concentration of 6.25 µg/mL (Sun et al., 2016).

Beside lethality, CuO-PEI NPs caused a high rate of malformed embryos starting from 5 µg/mL while CuO-PEG NPs were again completely ineffective even at a concentration ten times higher. These results highlighted that PEI coating worsens CuO NPs embryotoxicity. Instead, both ZnO-PEI and -PEG NPs caused to different degrees a significant percentage of malformed embryos at all tested concentrations (Fig. 5A). The 96 hpf EC50 values (Table 4) indicated that the potential of inducing malformations follows this order: PEI-CuO > PEI-ZnO > PEG-ZnO NPs. It is noteworthy that the ZnO-PEI NPs displayed a potential of inducing malformations five-fold higher than ZnO-PEG NPs, but the PEGylation is not able to completely countering the teratogenic

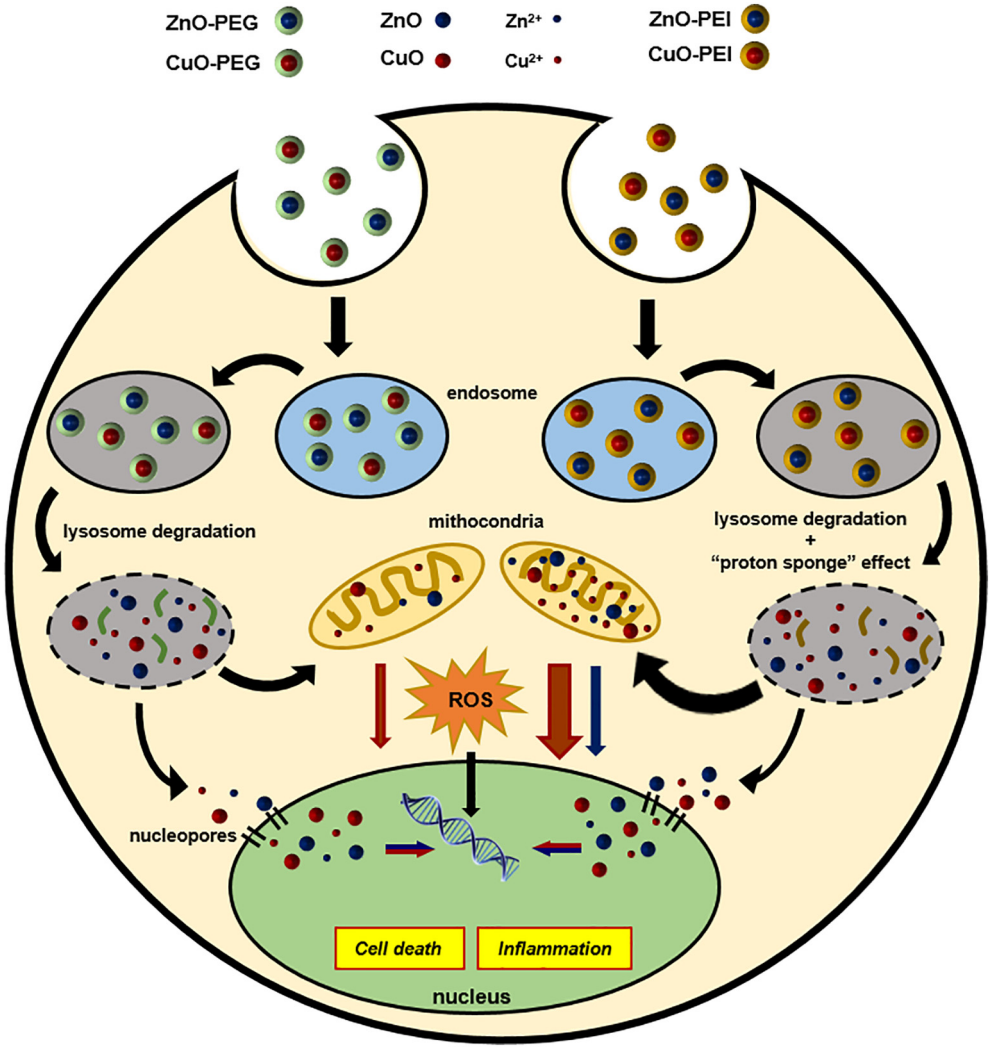

Scheme 1. Schematic representation of MeOs-PEI/PEG internalization and trafficking in A549 cells. Endocytosed NPs are degraded into lysosomes, and resulting uncoated NPs and free Cu^{2+} and Zn^{2+} interact with mitochondria and nucleus to exert their cytotoxic activity.

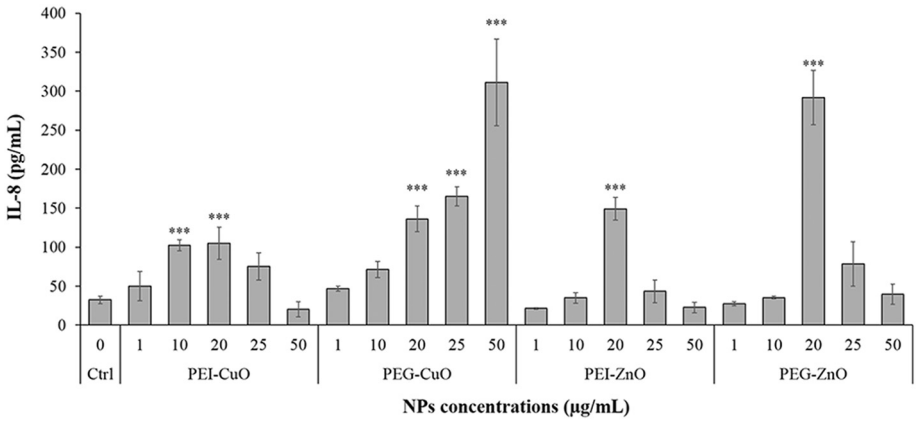

Fig. 4. Release of the pro-inflammatory cytokine IL-8 from A549 cells after 24 h exposure to CuO-PEG, CuO-PEI, ZnO-PEG and ZnO-PEI NPs at increasing concentrations (1–50 µg/mL), compared to untreated cells. Mean ± SE of 4 replicates for the NPs and 13 replicates for control (CTRL).***$p < 0.001$, *$p < 0.05$ vs. control (One-way ANOVA).

effect of ZnO NPs. This data is in agreement with one of our previous studies, in which PEG was able to reduce but not completely abolish the damage induced in embryos compared to nude commercial NP ZnO.11.

However, since for ZnO-PEG/PEI NPs it was not possible to estimate LC50 due to the low mortality at the concentrations tested, the teratogenic index (TI) was calculated only for PEI-CuO NPs. This TI is slightly higher than 1.5 and classifies PEI-CuO NPs as weakly teratogenic \(ASTM, 1998). In contrast, because the TI for PEI- and PEG-ZnO NPs results > 3, these NPs, although not embryolethal, could have a teratogenic potential .

Stereo microscopy observation allowed underscoring the incidence of single type of gross malformation in 96 hpf embryos (Fig. 6). Uncorrected gut coiling were recorded as predominant terata for PEG-ZnO treated embryos in agreement with our previous findings where gut was observed to be the main target organ of the different ZnO NPs tested (Bonfanti et al., 2015; Mantecca et al., 2015). In addition to this

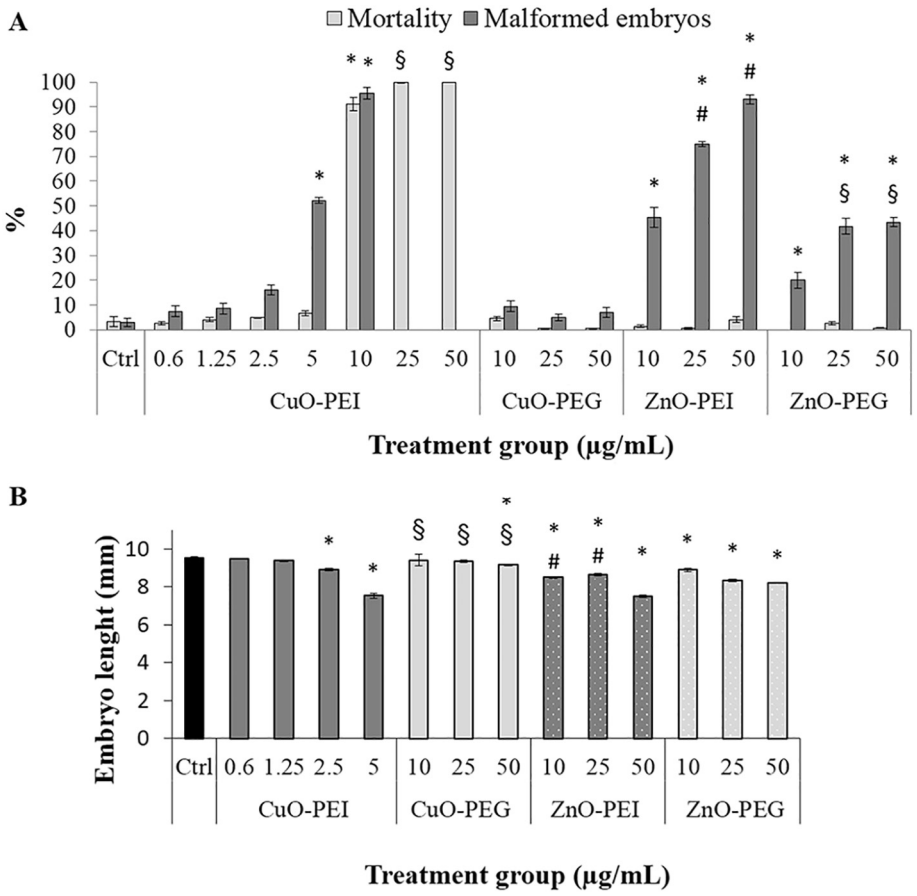

Fig. 5. Comparative embryotoxicity of CuO-PEI, CuO-PEG, ZnO-PEI and ZnO-PEG NPs in 96 hpf Xenopus embryos expressed as mortality and malformation rates (A) and head-tail length (B). All values are given as mean ± SE of three independent assays. *p < 0.01 vs control, §p < 0.01 vs the corresponding concentration of ZnO-PEI NPs, #p < 0.01 vs the corresponding concentration of CuO-PEG and ZnO-PEG respectively (One-way ANOVA + Fisher LSD Method).

Table 4
Comparative embryotoxicity of PEI and PEG coated CuO and ZnO NPs in 96 hpf *Xenopus laevis* embryos.

	96 hpf		
Treatment	LC50 (µg/mL)	EC50 (µg/mL)	TI
CuO-PEI	7.5 (6.9–7.9)	4.9 (4.4–5.6)	1.53
CuO-PEG	ND	ND	ND
ZnO-PEI	ND	12.1 (9.8–14.2)	ND
ZnO-PEG	ND	64.7 (43.9–153.9)	ND

ND = Not detectable.
LC50 = Median lethal concentration.
EC50 = Median teratogenic concentration.
TI = Teratogenic index (LC50/EC50).

abnormality, embryos treated with both the PEI coated NPs exhibited eye defects such as irregular pigmentation, optic cup ruptures, dislocation of the lens and incomplete closure of the choroid fissure, regardless of the type of metal oxide NPs (Fig. 6B). These phenotypes were worsened by diffuse edema and, particularly in 5 µg/mL CuO-PEI treated embryos, by severe tail flexures (Fig. 6A and B) as already observed in Xenopus embryos exposed to high concentrations of CuO NPs (Bacchetta et al., 2012).

Whole embryo cross sections has shown the detail of histological lesions in eyes, heart and intestine in PEI coated CuO and ZnO NPs (Fig. 7). The mild anomalies detected in eye region comprised a reduction of pigmented retina and a dislocation of lens in relation to optic cup in PEI-CuO embryos and thickness decrease of neural retina layers in PEI-ZnO embryos (Fig. 7, line A). The treatment also interfered with the development of the heart, altering the formation of cardiac chambers in particular in PEI-CuO NPs embryos, and reducing myocardial wall thickness and the formation of trabeculae in ZnO-PEI embryos (Fig. 7, line B). Finally, more severe injuries affected the abdominal region of treated embryos compromising the organ localization (Fig. 7, line C). The intestinal tube, usually characterized by multiple loops, appeared poorly coiled and the gut epithelium cells are still rich in vitelline platelets, indicating a delay in differentiation process. Furthermore, as already observed with the stereomicroscope, axial defects and edemas sometimes severe in the cephalic, cardiac and abdominal regions characterized the treated embryos.

To complete the FETAX endpoints, the embryo head-tail length was also measured, since embryo growth is often the most sensitive indicator of developmental toxicity (ASTM, 1998). According to this, the results showed that CuO-PEI NPs induced a significant growth inhibition compared to control group starting from 2.5 µg/mL, a concentration that was not effective in terms of mortality and malformations. In contrast, CuO-PEG NPs have not even affected this parameter. Instead, both PEI- and PEG-ZnO NPs reduced significantly the embryo length at all tested concentrations, with a stronger effect for ZnO-PEI NPs (Fig. 5B).

Even though growth reduction was previously evidenced as a recurring effect of nude ZnO NPs at concentrations ≥10 µg/mL both in Xenopus (Bacchetta et al., 2012; Bonfanti et al., 2015) and zebrafish embryos (Bai et al., 2010), only the PEI coating and not the PEG seems to worsen this damage.

Overall, the FETAX results showed that the embryotoxic profiles of CuO-PEI, CuO-PEG, ZnO-PEI and ZnO-PEG are markedly influenced by surface coating but also depend on the type of metal oxide NPs. PEI was found to be an unsafe coating compared to PEG for both tested NPs, although this is particularly pronounced for CuO NPs. As already demonstrated with a branched PEI in *Xenopus laevis* embryos (Colombo et al., 2017) and with a PEI 25 KDa in zebrafish embryos,36 the polymer itself can disrupt early development probably due to its

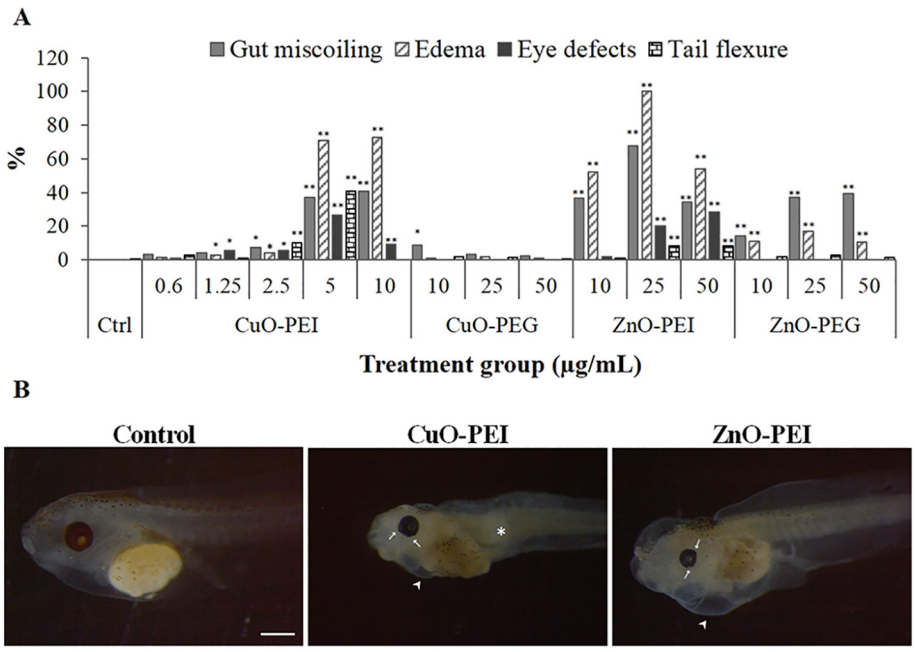

Fig. 6. Malformation pattern in 96 hpf Xenopus embryos caused by 96 h exposure to PEI and PEG coated CuO and ZnO NPs compared to control (Ctrl). Recurrent and not sporadic malformation percentages (A). All values are given as mean ± SE of three independent assays. *p < 0.05 vs control, **p < 0.01 vs control (One-way ANOVA + Fisher LSD Method). Representative lateral view of control, PEI-CuO NPs (5 µg/mL) and PEI-ZnO NPs (25 µg/mL) treated embryos (B). Arrows: eye defects; arrowhead: cardiac edema; asterisk: tail flexure. Bar: 500 µm.

cationic nature which facilitates its interaction with biological membranes. This could explain the specific ocular and cardiac defects that have appeared in embryos treated with both PEI coated NPs. Indeed, cardiovascular toxicity and downregulation of heart development related genes have been shown in zebrafish embryos treated with PEI 25 KDa (Hu et al., 2017).

Another reason why CuO-PEI and ZnO-PEI NPs have a higher embryotoxic potential than the corresponding PEG-coated NPs resides in the ability of PEI to deliver nanomaterials to cells as above described. This concept is validated by studies on zebrafish embryos in which it has been demonstrated that PEI-mesopouros silica nanoparticles penetrate into the organs displaying higher toxicity than the same NPs functionalized with PEG that remain aggregated on the skin surface (Paatero et al., 2017). Moreover, PEG was proposed as a model molecule to add stealth properties to therapeutic NPs as PEG coated NPs showed greater persistence in the bloodstream and lower affinity for endothelium after injection in zebrafish embryos (Evensen et al., 2016). To highlight whether the two coating agents could vehicle differently NPs, ICP-OES analysis of Cu and Zn content in embryonic tissues was performed. As for in vitro assays, no statistically significant differences in Cu and Zn bioaccumulation between the respective PEI and PEG coated NPs were evidenced (Fig. S2). Therefore, in line with the mechanism described for A549 (Scheme 1), PEI seems to ehnance endosomal escape through the proton sponge effect also in Xenopus embryos and facilitate the release into the cytoplasm of enterocytes more than PEG-coated NPs.

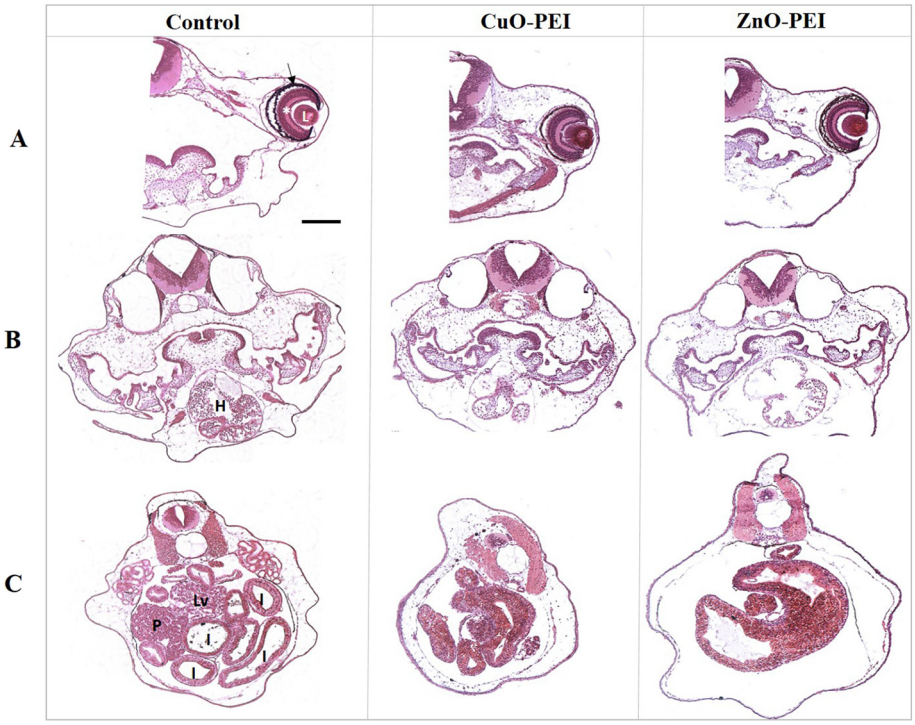

Fig. 7. Histological transversal sections 96 hpf Xenopus embryos at level of eye (line A), heart (line B), abdominal (line C) regions. Note the altered morphology and localization of primitive organs in the treated embryos compared to control. Arrow: tapetum nigrum; asterisk: neural retina; L: lens; Lv: liver; P: pancreas; I: intestine. Bar: 200 µm.

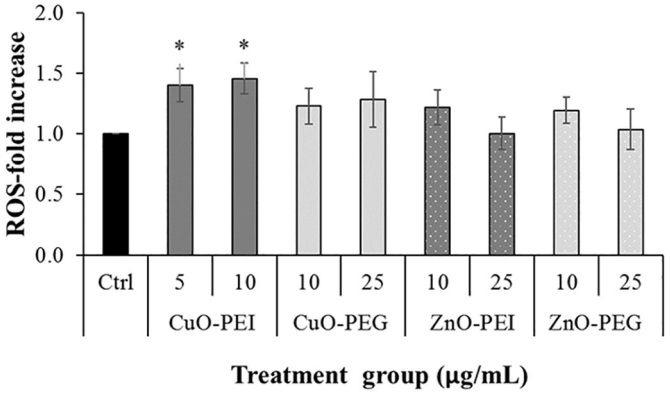

Fig. 8. ROS fold-increase in 96 hpf Xenopus embryos treated with PEI and PEG coated CuO and ZnO NPs compared to control (Ctrl). All values are given as mean ± SE of three independent assays. *p < 0.05 vs control (Student *t*-test).

Looking at our results, a statistically increase of ROS levels with respect to control was highlighted only in PEI-CuO treated embryos at both 5 and 10 µg/mL (Fig. 8). This result is particularly valuable for the developing Xenopus, which are provided of a good antioxidant defenses such as SOD and the GSH-related system, able to buffer ROS production (Rizzo et al., 2007). Since oxidative stress is recognized as the main mechanism triggering metal oxide NP toxicity across many test species (Bondarenko et al., 2013), this ROS increment could be the reason for the high embryolethality of the CuO-PEI NPs. In contrast, the specific teratogenicity of ZnO NPs would be related mainly to the metal oxide NPs themselves accordingly with our previous papers and in this case the polymeric coatings could act by modulating their interaction with the embryonic tissues.

3. Conclusions

In summary, the present work is aimed to define new strategies to reduce the well-known toxicity of MeOs antibacterial NPs, by coating the surface with different polymeric shells. The overall results obtained on lung cells and Xenopus embryos indicate that PEG coating is able to exert a protective function against CuOs and, in a lower extent, ZnOs NPs toxicity. On the other hand, PEI is not a suitable coating material for producing safe MeONPs due to its inability to prevent adverse effect both in vitro and on developing vertebrates. The higher intracellular availability of MeOs and derived ions upon PEI-mediated internalization seems responsible for the non-protective role of this polymer respect to PEG. PEI coating might be rather taken into consideration and exploited for the design of new drugs with enhanced cytotoxicity.

The in vitro results confirmed that functionalized MeOs toxicity involves ROS-dependent and -independent mechanisms, which are ultimately responsible of the different outcome on lung cell viability, and *Xenopus laevis* embryos lethality and malformations.

Finally, our study provides robust evidence of how the integration between standard in vitro assays and alternative approaches on developing organisms represents a powerful tool for screening NP-induced toxicities. The early developmental vertebrates are ideal alternative models to be combined with standardized safety in vitro protocols, with the benefit of reducing time and cost of mammalian models. Further investigations are mandatory in order to described even better and in detail how secondary MPs can influence the aquatic organism behaviour and fitness.

4. Materials and methods

4.1. Characterization of NPs suspension

The Dynamic Light Scattering (DLS) was used to characterize the hydrodynamic behavior of the nanocolloid suspensions. The samples were diluted to a final concentration of 50 µg/L, in MQ water, Fetax solution and in Opti-MEM (Gibco, Life Technology, Italy) supplemented with 1% fetal bovine serum (FBS). Both the hydrodynamic dimension and superficial charge of the nanocolloids were expressed as mean ± ES.

4.2. Cell viability

Human alveolar epithelial cells A549 (ATCC®CCL-185™), were routinely maintained in Opti-MEM medium with 10% FBS and 1% penicillin/streptomycin and were grown at 37 °C, 5% CO_2 and controlled humidity. Cells were seeded in 6 multi-well plates (1.8 × 105 cells/well) and, upon reaching the confluence, exposed for 3 and 24 h to nanocolloids suspensions (1 µg/mL-50 µg/mL) in 1% FBS supplemented medium. Untreated cells were used as control. At the end of the treatment, supernatants were removed and stored at −20 °C for further analysis, cells were rinsed and MTT [3-(4,5-dimethylthiazol-2-yl)-25-diphenyltetrazolium bromide] solution was added in the medium for 2 h. Thereafter, the formazan crystals were solubilized in 1 mL DMSO and the absorbance of each sample, proportional to cell viability, was measured with a multimode microplate reader (Infinite® M200 PRO, Tecan) at 570 nm using 690 nm as reference wavelength. Cell viability was expressed as OD mean percent compared to untreated cells.

4.3. ICP measurement of ions release in culture medium

The amount of Cu^{2+} and Zn^{2+} released by the four NP types in A549 medium, was measured by incubating 20 µg/mL NPs in Opti-MEM medium with 10% FBS and 1% penicillin/streptomycin at 37 °C, 5% CO_2 and controlled humidity. After 24 h, the medium samples were collected, filtrated by centrifugation in Vivaspin 10 KD (Sartorius), in order to separate the free ions, and the filtrated solutions were analyzed by ICP-OES (PerkinElmer, Optima 7000 DV Perkin Elmer). To determine the percentage of released ions respect to the total amount of ions in medium samples, unfiltered solutions have been also measured by ICP, after digestion in HNO3 5%. Measurements were repeated three times on different embryo pools.

4.4. ROS analysis in A549 cells

Before treatment with nanocolloids, cells were incubated at 37 °C for 20 min in the dark with 10 µM of the oxidation-sensitive fluorescence probe 2′-7′-dichlorofluorescein diacetate (DCFH-DA) (Zhao et al., 2013). The probe was used to measure the levels of intracellular reactive oxygen species (ROS) by measuring the fluorescence intensity of dichlorofluorescein (DCF), the ROS oxidation product of dichlorodihydrofluorescein (DFCH). After the incubation cells were washed twice and exposed to 20–50 µg/mL of each nanocolloid suspension for 3 or 6 h. Cells untreated were used as negative control whereas positive control cells were exposed to 5 mM of hydrogen peroxide. Ultimately, cells were washed again, detached and centrifuged, the pellets were than suspended in PBS 1× and the ROS levels were determined by flow cytometry (CytoFLEX, Beckman Coulter). Intracellular ROS levels were expressed as fold change compared to untreated cells.

4.5. IL-8 assays

To measure the pro-inflammatory response to each treatment, the collected cells supernatants were tested in order to verify the interleukin-8 (IL-8) levels released by the cells. The Human IL-8 CytosetTM kit (InvitrogenTM) was used to perform the assays following the manufacturer protocol while the extracellular IL-8 levels of each sample were expressed in pg/mL.

4.6. Frog embryo teratogenesis assay-xenopus (FETAX)

Embryotoxicity tests were conducted according to the standard guide for the Frog Embryo Teratogenesis Assay–Xenopus (FETAX)33 with minor modification. Embryos were obtained by natural breeding of pairs of adult *Xenopus laevis* as previously described (Bonfanti et al., 2018), and used up to 96 h post-fertilization (hpf). During this period embryos are not independently feeding and therefore outside the scope of the directive 2010/63/EU on the protection of the animals used for scientific purposes. After breeding, embryos at two or four blastomeres were collected and the jelly coat was removed by swirling the embryos for 1–2 min in a 2.25%L-cysteine solution (pH 8.1).

In order to compare the embryotoxic effects of to nanocolloids suspensions, at least three replicate definitive tests in the same experimental conditions were performed. Normally-cleaved embryos at the midblastula stage (Stage 8), 5 hpf (Niieukoop and Faber, 1994), were selected for testing and groups of 25 embryos from each male/female pair ($n = 3$) were randomly placed in covered 6.0 cm Petri dishes containing 10 mL of control or test solution. Two replicate dishes were used for each test concentration (PEI-CuO 0.6–10 μg/mL, PEG-CuO, PEI and PEG-ZnO 10–50 μg/mL freshly prepared in FETAX solution), while for control group four replicate dishes were used. All of the Petri dishes were incubated in a thermostatic chamber at 23 ± 0.5 °C until the end of the test (96 hpf, Stage 46). Every day, exposure solutions were changed and dead embryos recorded and removed.

At the end of the test, all the embryos (Stage 46) were anesthetized with 100 mg/L MS-222 and screened for single morphological abnormalities under a dissecting microscope (Zeiss, Germany). Three pools of embryos from each experimental group of each definitive test were selected and randomly processed for morphological and biochemical analysis. To estimate the growth retardation, head–tail length of formalin fixed embryos was measured by the digitizing software AxioVision. To evaluate histological alterations, embryos were fixed in Bouin's solution and processed for paraffin embedding. To measure ROS production, the embryos were immediately stored at −80 °C until use.

4.7. Histopathological analysis in embryos

For light microscopy analyses, embedded stage 46 embryos ($n = 15$ from PEI-CuO 5 μg/mL and PEI-ZnO 25 μg/mL) were transversely cut from eye to proctodeum into serial sections 6 μm thick, then mounted on glass slides and stained with hematoxylin and eosin (H&E). The sections were finally examined at light microscope (Zeiss Axioplan) equipped with a digital camera (Axiocam MRc5).

4.8. ROS analysis in embryos

ROS generation in stage 46 embryos exposed to nanocolloids for the duration of FETAX assay were measured according to Zhao et al. (2013) using DCFH-DA.41 Briefly, pools of 10 embryos were homogenized in 1 mL PBS (pH = 7.4) at 4 °C and the homogenates were centrifuged at 12,000 ×*g* for 30 min at 4 °C in a mini-centrifuge (Eppendorf 5415C). Twenty μL of the collected supernatants were incubated at room temperature (RT) for 5 min in a 96-well plate and then 100 μL PBS and 8.3 μL DCFH-DA stock solution (10 mg/mL in DMSO) were added to each well. After incubation at RT for 30 min in the dark, the fluorescence intensity was measured using a micro plate reader (Tecan, infinite M200PRO) with excitation and emission wavelengths of 485 and 530 nm, respectively. After quantification of proteins (Bradford, 1976), ROS concentration was calculated in arbitrary units (dichlorofluorescein/mg proteins).

4.9. Cu and Zn bioaccumulation in A549 cells and embryos

For the determination of Cu and Zn accumulation in A549 cells, the cells were incubated for 24 h with 20 μg/mL CuO-PEI, CuO-PEG, ZnO-PEI and ZnO-PEG. At the end of incubation, the cells were counted, centrifuged for 6 min at 1200 rpm and the pellet suspended in PBS to be processed for ICP-OES analysis. For the determination of Cu and Zn bioaccumulation in Xenopus embryos, at the end of FETAX test, 50 embryos from each experimental group were randomly collected in Petri dishes containing fresh FETAX solution for 24 h for purging from ingested NPs. Embryos were then quickly frozen on dry ice and stored at −80 °C until analyses. Then, embryos were completely dried at 40 °C and the dry mass registered with a microbalance.

Cells and embryos samples were then digested in 4 mL of 65% HNO3 using a mineralizator (Milestone Ethos TC, Milestone srl, Italy), diluted and then analyzed by ICP-OES. All measurements were repeated three times. The values obtained by the analysis on A549 samples were expressed as μg/mL $x10^6$, normalized on the n° of cells at the end of incubation. The values obtained by the analyses on embryos were expressed as.

4.10. Statistical analysis

EC50 values (μg/mL) for cell viability assay (EC50: effective concentration of compound decreasing cell viability by 50%) were elaborated by Probit analysis and expressed as Mean ± SD. The results obtained by ROS and IL-8 release assays were expressed as Mean ± SE and compared using one-way ANOVA.

In FETAX test, the data were tested for homogeneity and normality. When these assumptions were met, one-way ANOVA was performed; otherwise, the non-parametric Kruskal–Wallis test was applied. The significance level was set at $p < 0.05$. The incidence of specific malformations was investigated by chi-square method, using Yates's correction for continuity ($\chi 2$ test) or Fisher's exact tests (FE test). Mortality and malformation percentages were used to calculate the 96 hpf LC50 (concentration causing 50% lethality) and 96 hpf EC50 (concentration inducing teratogenesis in 50% of surviving embryos) for each experimental group. These values were obtained following the elaboration of the lethality and malformation percentages by the Probit analysis (Finney, 1971), using the U.S. EPA Probit Analysis Program, Version 1.5, with 95% confidence interval. The Teratogenic Index (TI), useful in estimating the teratogenic risk associated with the tested compounds, is represented by the LC50/EC50 ratio. ROS values, expressed as fold change compared to untreated embryos ± SE, and the bioaccumulation values, given as mean ± SE, were compared by one-way ANOVA.

For all statistical comparisons, $p < 0.05$ was considered significant.

Funding sources

This work was supported by the European project PROTECT, “Pre-commercial lines for production of surface nanostructured antimicrobial and anti-biofilm textiles, medical devices and water treatment membranes (H2020-720851) (www.protect-h2020.eu).

Aknowledgements

We thank Dr. Tiziano Catelani and “Piattaforma Interdipartimentale di Microscopia” of University of Milan – Bicocca for TEM images.

Declaration of competing interest

The authors declare that they have no conflict of interests.

Appendix A. Supplementary data

Supplementary data to this article can be found online at https://doi.org/10.1016/j.impact.2019.100195.

References

Akhtar, M.J., Kumar, S., Alhadlaq, H.A., Alrokayan, S.A., Abu-Salah, K.M., Ahamed, M., 2016. Dose-dependent genotoxicity of copper oxide nanoparticles stimulated by reactive oxygen species in human lung epithelial cells. Toxicol. Ind. Health 32, 809–821. https://doi.org/10.1177/0748233713511512.

Azam, A., Ahmed, A.S., Oves, M., Khan, M.S., Habib, S.S., Memic, A., 2012. Antimicrobial activity of metal oxide nanoparticles against Gram-positive and Gram-negative bacteria: a comparative study. Int. J. Nanomedicine 7, 6003. https://doi.org/10.2147/IJN.S35347.

Bacchetta, R., Santo, N., Fascio, U., Moschini, E., Freddi, S., Chirico, G., Camatini, M., Mantecca, P., 2012. Nano-sized CuO, TiO $_2$ and ZnO affect *Xenopus laevis* development. Nanotoxicology 6, 381–398. https://doi.org/10.3109/17435390.2011.579634.

Bacchetta, R., Moschini, E., Santo, N., Fascio, U., Del Giacco, L., Freddi, S., Camatini, M., Mantecca, P., 2013. Evidence and uptake routes for zinc oxide nanoparticles through the gastrointestinal barrier in *Xenopus laevis*. Nanotoxicology 8, 1–17. https://doi.org/10.3109/17435390.2013.824128.

Bai, W., Zhang, Z., Tian, W., He, X., Ma, Y., Zhao, Y., Chai, Z., 2010. Toxicity of zinc oxide nanoparticles to zebrafish embryo: a physicochemical study of toxicity mechanism. J. Nanopart. Res. 12, 1645–1654. https://doi.org/10.1007/s11051-009-9740-9.

Behr, J.P., 1997. The proton sponge. A trick to enter cells the viruses did not exploit. Chimia (Aarau). 51, 34–36.

Bondarenko, O., Juganson, K., Ivask, A., Kasemets, K., Mortimer, M., Kahru, A., 2013. Toxicity of Ag, CuO and ZnO nanoparticles to selected environmentally relevant test organisms and mammalian cells in vitro: a critical review. Arch. Toxicol. 87, 1181–1200. https://doi.org/10.1007/s00204-013-1079-4.

Bonfanti, P., Moschini, E., Saibene, M., Bacchetta, R., Rettighieri, L., Calabri, L., Colombo, A., Mantecca, P., 2015. Do nanoparticle physico-chemical properties and developmental exposure window influence nano ZnO embryotoxicity in Xenopus laevis? Int. J. Environ. Res. Public Health 12, 8828–8848. https://doi.org/10.3390/ijerph120808828.

Bonfanti, P., Saibene, M., Bacchetta, R., Mantecca, P., Colombo, A., 2018. A glyphosate micro-emulsion formulation displays teratogenicity in Xenopus laevis. Aquat. Toxicol. 195, 103–113. https://doi.org/10.1016/j.aquatox.2017.12.007.

Bradford, MM., 1976. A rapid and sensitive method for the quantitation of microgram quantities of protein utilizing the principle of protein-dye binding. Anal Biochem 72, 248–254.

Cai, X., Lee, A., Ji, Z., Huang, C., Chang, C.H., Wang, X., Liao, Y.-P., Xia, T., Li, R., 2017. Reduction of pulmonary toxicity of metal oxide nanoparticles by phosphonate-based surface passivation. Part. Fibre Toxicol. 14, 13. https://doi.org/10.1186/s12989-017-0193-5.

Chang, Y.-N., Zhang, M., Xia, L., Zhang, J., Xing, G., 2012. The toxic effects and mechanisms of CuO and ZnO nanoparticles. Materials (Basel). 5, 2850–2871. https://doi.org/10.3390/ma5122850.

Colombo, A., Saibene, M., Moschini, E., Bonfanti, P., Collini, M., Kasemets, K., Mantecca, P., 2017. Teratogenic hazard of BPEI-coated silver nanoparticles to *Xenopus laevis*. Nanotoxicology 11, 405–418. https://doi.org/10.1080/17435390.2017.1309703.

Evensen, L., Johansen, P.L., Koster, G., Zhu, K., Herfindal, L., Speth, M., Fenaroli, F., Hildahl, J., Bagherifam, S., Tulotta, C., Prasmickaite, L., Mælandsmo, G.M., Snaar-Jagalska, E., Griffiths, G., 2016. Zebrafish as a model system for characterization of nanoparticles against cancer. Nanoscale 8, 862–877. https://doi.org/10.1039/C5NR07289A.

Finney, D.J., 1971. Probit Analysis. J. Pharm. Sci. 60, 1432. https://doi.org/10.1002/jps.2600600940.

Ganesan, S., Anaimalai Thirumurthi, N., Raghunath, A., Vijayakumar, S., Perumal, E., 2016. Acute and sub-lethal exposure to copper oxide nanoparticles causes oxidative stress and teratogenicity in zebrafish embryos. J. Appl. Toxicol. 36, 554–567. https://doi.org/10.1002/jat.3224.

He, X., Hwang, H.-M., 2016. Nanotechnology in food science: functionality, applicability, and safety assessment. J. Food Drug Anal. 24, 671–681. https://doi.org/10.1016/J.JFDA.2016.06.001.

Hou, J., Wang, Xiangxue, Hayat, T., Wang, Xiangke, 2017. Ecotoxicological effects and mechanism of CuO nanoparticles to individual organisms. Environ. Pollut. 221, 209–217. https://doi.org/10.1016/j.envpol.2016.11.066.

Hu, Q., Guo, F., Zhao, F., Tang, G., Fu, Z., 2017. Cardiovascular toxicity assessment of poly (ethylene imine)-based cationic polymers on zebrafish model. J. Biomater. Sci. Polym. Ed. 28, 768–780. https://doi.org/10.1080/09205063.2017.1301773.

Ivask, A., Juganson, K., Bondarenko, O., Mortimer, M., Aruoja, V., Kasemets, K., Blinova, I., Heinlaan, M., Slaveykova, V., Kahru, A., 2014. Mechanisms of toxic action of Ag, ZnO and CuO nanoparticles to selected ecotoxicological test organisms and mammalian cells in vitro: a comparative review. Nanotoxicology 8 (Suppl. 1), 57–71. https://doi.org/10.3109/17435390.2013.855831.

Kadiyala, U., Kotov, N.A., Van Epps, J.S., 2018. Antibacterial metal oxide nanoparticles: challenges in interpreting the literature. Curr. Pharm. Des. 24, 896–903. https://doi.org/10.2174/1381612824666180219130659.

Khanna, P., Ong, C., Bay, B., Baeg, G., 2015. Nanotoxicity: an interplay of oxidative stress, inflammation and cell death. Nanomaterials 5, 1163–1180. https://doi.org/10.3390/nano5031163.

Kumari, P., Panda, P.K., Jha, E., Kumari, K., Nisha, K., Mallick, M.A., Verma, S.K., 2017. Mechanistic insight to ROS and apoptosis regulated cytotoxicity inferred by green synthesized CuO nanoparticles from Calotropis gigantea to embryonic zebrafish. Sci. Rep. 7, 16284. https://doi.org/10.1038/s41598-017-16581-1.

Kung, M.-L., Hsieh, S.-L., Wu, C.-C., Chu, T.-H., Lin, Y.-C., Yeh, B.-W., Hsieh, S., 2015. Enhanced reactive oxygen species overexpression by CuO nanoparticles in poorly differentiated hepatocellular carcinoma cells. Nanoscale 7, 1820–1829. https://doi.org/10.1039/c4nr05843g.

Lenz, A.G., Karg, E., Brendel, E., Hinze-Heyn, H., Maier, K.L., Eickelberg, O., Stoeger, T., Schmid, O., 2013. Inflammatory and oxidative stress responses of an alveolar epithelial cell line to airborne zinc oxide nanoparticles at the air-liquid interface: a comparison with conventional, submerged cell-culture conditions. Biomed. Res. Int. 2013. https://doi.org/10.1155/2013/652632.

Liu, J., Kang, Y., Yin, S., Song, B., Wei, L., Chen, L., Shao, L., 2017. Zinc oxide nanoparticles induce toxic responses in human neuroblastoma SHSY5Y cells in a size-dependent manner. Int. J. Nanomedicine. https://doi.org/10.2147/IJN.S149070.

Mantecca, P., Moschini, E., Bonfanti, P., Fascio, U., Perelshtein, I., Lipovsky, A., Chirico, G., Bacchetta, R., Del Giacco, L., Colombo, A., Gedanken, A., 2015. Toxicity evaluation of a new Zn-doped CuO nanocomposite with highly effective antibacterial properties. Toxicol. Sci. 146, 16–30. https://doi.org/10.1093/toxsci/kfv067.

Mantecca, P., Kasemets, K., Deokar, A., Perelshtein, I., Gedanken, A., Bahk, Y.K., Kianfar, B., Wang, J., 2017. Airborne nanoparticle release and toxicological risk from metal-oxide-coated textiles: toward a multiscale safe-by-design approach. Environ. Sci. Technol. 51, 9305–9317. https://doi.org/10.1021/acs.est.7b02390.

Marín-Barba, M., Gavilán, H., Gutiérrez, L., Lozano-Velasco, E., Rodríguez-Ramiro, I., Wheeler, G.N., Morris, C.J., Morales, M.P., Ruiz, A., 2018. Unravelling the mechanisms that determine the uptake and metabolism of magnetic single and multicore nanoparticles in a Xenopus laevis model. Nanoscale 10, 690–704. https://doi.org/10.1039/c7nr06020c.

Midander, K., Cronholm, P., Karlsson, H.L., Elihn, K., Möller, L., Leygraf, C., Wallinder, I.O., 2009. Surface characteristics, copper release, and toxicity of nano- and micrometer-sized copper and copper (II) oxide particles: a cross-disciplinary study. Small 5, 389–399. https://doi.org/10.1002/smll.200801220.

Nagvenkar, A.P., Deokar, A., Perelshtein, I., Gedanken, A., 2016. A one-step sonochemical synthesis of stable ZnO–PVA nanocolloid as a potential biocidal agent. J. Mater. Chem. B 4, 2124–2132. https://doi.org/10.1039/C6TB00033A.

Nagvenkar, A.P., Perelshtein, I., Piunno, Y., Mantecca, P., Gedanken, A., 2019. Sonochemical one-step synthesis of polymer-capped metal oxide nanocolloids: antibacterial activity and cytotoxicity. ACS Omega. https://doi.org/10.1021/acsomega.9b00181.

Nations, S., Wages, M., Cañas, J.E., Maul, J., Theodorakis, C., Cobb, G.P., 2011. Acute effects of Fe2O3, TiO2, ZnO and CuO nanomaterials on Xenopus laevis. Chemosphere 83, 1053–1061. https://doi.org/10.1016/j.chemosphere.2011.01.061.

Nieuwkoop, P.D., Faber, J., 1994. Normal Table of *Xenopus laevis* (Daudin): A Systematical and Chronological Survey of the Development From the Fertilized Egg Till the End of Metamorphosis. Garland Pub, New York.

Osmond McLeod, M.J., Oytam, Y., Osmond, R.I., Sobhanmanesh, F., McCall, M.J., 2014. Surface coatings protect against the in vitro toxicity of zinc oxide nanoparticles in human hepatic stellate cells. J. Nanomed. Nanotechnol. 05. https://doi.org/10.4172/2157-7439.1000232.

Paatero, I., Casals, E., Niemi, R., Özliseli, E., Rosenholm, J.M., Sahlgren, C., 2017. Analyses in zebrafish embryos reveal that nanotoxicity profiles are dependent on surface-functionalization controlled penetrance of biological membranes. Sci. Rep. 7, 8423. https://doi.org/10.1038/s41598-017-09312-z.

Perelshtein, I., Lipovsky, A., Perkas, N., Gedanken, A., Moschini, E., Mantecca, P., 2015a. The influence of the crystalline nature of nano-metal oxides on their antibacterial and toxicity properties. Nano Res. 8, 695–707. https://doi.org/10.1007/s12274-014-0553-5.

Perelshtein, I., Lipovsky, A., Perkas, N., Tzanov, T., Arguirova, M., Leseva, M., Gedanken, A., 2015b. Making the hospital a safer place by sonochemical coating of all its textiles with antibacterial nanoparticles. Ultrason. Sonochem. 25, 82–88. https://doi.org/10.1016/j.ultsonch.2014.12.012.

Rejman, J., Bragonzi, A., Conese, M., 2005. Role of clathrin- and caveolae-mediated endocytosis in gene transfer mediated by lipo- and polyplexes. Mol. Ther. 12, 468–474. https://doi.org/10.1016/j.ymthe.2005.03.038.

Rizzo, A.M., Adorni, L., Montorfano, G., Rossi, F., Berra, B., 2007. Antioxidant metabolism of Xenopus laevis embryos during the first days of development. Comp. Biochem. Physiol. Part B Biochem. Mol. Biol. 146, 94–100. https://doi.org/10.1016/j.cbpb.2006.09.009.

Sahu, D., Kannan, G.M., Vijayaraghavan, R., Anand, T., Khanum, F., 2013. Nanosized zinc oxide induces toxicity in human lung cells. ISRN Toxicol. 2013, 316075. https://doi.org/10.1155/2013/316075.

Scherzad, A., Meyer, T., Kleinsasser, N., Hackenberg, S., 2017. Molecular mechanisms of zinc oxide nanoparticle-induced genotoxicity short running title: genotoxicity of ZnO NPs. Materials (Basel). 10, 1427. https://doi.org/10.3390/ma10121427.

ASTM, 1998. American Society for Testing and Materials. Standard guide for conducting the Frog Embryo Teratogenesis Assay-Xenopus E-1439–E1498..

Sun, Y., Zhang, G., He, Z., Wang, Y., Cui, J., Li, Y., 2016. Effects of copper oxide nanoparticles on developing zebrafish embryos and larvae. Int. J. Nanomedicine 905. https://doi.org/10.2147/IJN.S100350.

Van Teunenbroek, T., 2016. NANoREG-A common European approach to the regulatory testing of nanomaterials (part 1).

Wang, Z., Li, N., Zhao, J., White, J.C., Qu, P., Xing, B., 2012. CuO nanoparticle interaction with human epithelial cells: cellular uptake, location, export, and genotoxicity. Chem. Res. Toxicol. 25, 1512–1521. https://doi.org/10.1021/tx3002093.

Zhao, X., Wang, S., Wu, Y., You, H., Lv, L., 2013. Acute ZnO nanoparticles exposure induces developmental toxicity, oxidative stress and DNA damage in embryo-larval zebrafish. Aquat. Toxicol. 136–137, 49–59. https://doi.org/10.1016/j.aquatox.2013.03.019.